A New 3-D FDTD Multigrid Technique with Dielectric Traverse Capabilities

Mikel J. White, *Member, IEEE*, Zhengqing Yun, *Member, IEEE*, and Magdy F. Iskander, *Fellow, IEEE*

***Abstract*—The finite-difference time-domain (FDTD) technique has become increasingly popular and is being used to model extremely complex and electrically large structures. These simulations are computationally demanding and often exceed available limits on computer resources. In this paper, we present an FDTD sub-gridding technique that allows for increased resolution in regions of interest without increasing the overall computational requirements beyond the available resources. Furthermore, the formulation presented here allows for traversing dielectric boundaries using any integer refinement factor and the maximum Courant number. By allowing the coarse-/fine-grid boundary to traverse dielectric boundaries, numerical simulations that were previously either extremely difficult or impossible to perform are now possible. The technique presented here uses a weighted current value from the coarse region at the boundary between the fine- and coarse-grid regions to update the fine-region tangential fields on that boundary. The weighting function depends on the material properties and the relative position of the fine-region electric field within the current contour at the boundary. The complete formulation of this new technique is described and some results of simulation cases are presented to validate the accuracy and stability of the newly developed FDTD code. Simulations include simple cases where the analytical solution exists and more complex cases, which were impossible to model using a uniform-grid FDTD code. In some simulation examples, computer memory savings as high as 70 times what would have been necessary with a uniform-grid code were achieved. It is shown that errors of less than 2% are achievable with ratios of coarse-to-fine grid sizes exceeding ten. The new technique is expected to be used in simulating many electrically large and complex structures in the biomedical microwave processing of materials and the wireless communications areas.**

***Index Terms*—Complex structures, dielectric traverse, electrically large, finite-difference time-domain method, multigrid, sub-gridding.**

I. Introduction

IT IS generally known that the finite-difference time-domain (FDTD) method is a powerful numerical technique suitable for analyzing a wide variety of electromagnetic-field problems. As this technique has grown in popularity, a desire to model more complex structures has created a need to improve the memory and computational time requirements of the FDTD method due to often-limited available computer resources. Examples of numerical modeling projects that often require extensive computational resources include: 1) simulation of via's and bond wires in high-frequency electronic packages; 2) detailed simulation of biomedical applications; and 3) materials processing in multimode microwave cavities. It is also often desirable to more accurately model circular structures using the stair-step approximation inherent in the FDTD technique. To this end, we devised a new technique for sub-gridding the FDTD technique, which increases the resolution in regions of interest.

Recently, our group published a paper that detailed a new method of sub-gridding the FDTD technique [1]. This technique, however, did not allow the fine/coarse interface boundary (henceforth referred to as the interface boundary) to traverse dielectric boundaries. Unlike the previous method, the technique presented here is stable and produces accurate results when sub-gridding at a dielectric boundary. Even when the interface boundary does not traverse a dielectric boundary, the technique presented here proves accurate and stable. Using previous sub-gridding techniques, it was often required to make the fine-grid region extremely large so that the interface boundary did not cross any dielectric boundaries. In many simulations, this is impractical due to the physical structure of the model. For example, in microwave sintering experiments, the samples are typically placed on a ceramic shelf. This shelf often extends the entire length and width of the cavity. In such a simulation, it is impossible to place the interface boundary around the region of interest (i.e., the sample) without traversing a dielectric boundary. Therefore, previous sub-gridding techniques may not be used and a procedure for traversing dielectric boundaries is required. The technique presented here is general and allows the interface boundary to traverse dielectric boundaries and may, therefore, be used in the effective simulation of this and similar problems.

Other methods have been described for sub-gridding the FDTD method, including: 1) the variable step-size method (VSSM) [2]; 2) the mesh-refinement algorithm (MRA) [3]; 3) a pulsed sub-gridding algorithm [4]; and 4) the multigrid displacement method (MGDM) [1] published by our group. The MGDM is, in fact, a three-dimensional (3-D) extension of the MRA method. In [1], it was shown that the MGDM performed better than the VSSM when modeling complex 3-D structures. However, neither method allowed for traversing dielectric boundaries. Chevalier and Luebbers in a recent paper described a sub-gridding technique that allows for material traverse [5]. This technique, however, works only for odd-integer refinement factors. In fact, results in [5] were presented only for a refinement factor of three. Therefore, the technique presented here is considered to be the most general available method since it works for any refinement factor, odd or even, and was tested for integer refinement factors larger than ten. Furthermore, it is possible to use a Courant number of 0.57 for the 3-D simulations using the developed technique. To simplify the explanation, we consider only the case of an equal-sided cubic grid. However, the present technique is applicable for any rectangular grid.

Manuscript received August 31, 1999.

The authors are with the Department of Electrical Engineering, University of Utah, Salt Lake City, UT 84112 USA.

Publisher Item Identifier S 0018-9480(01)01676-3.

II. Sub-Gridding the FDTD Technique

The sub-gridding technique is based on creating two separate regions: a coarse-grid region and a fine-grid region surrounding the area of interest inside the coarse-grid region. In order to keep the derivation of the code and the code itself relatively simple, the fine-grid region is made an integer fraction of the coarse grid. Thus, if the coarse-grid cell size (cubical) is $\Delta\ell_c$ and the fine-grid cell size is $\Delta\ell_f$, then the integer refinement factor $n\text{fact}$ may be written as

$$n\text{fact} = \frac{\Delta\ell_c}{\Delta\ell_f}. \tag{1}$$

The coarse-grid region is iterated over once, and then the fine region is iterated over $n\text{fact}$ times using the normal FDTD update equations. In order to transfer information from the coarse-grid to the fine-grid region, the tangential electric fields of the fine grid on the interface boundaries must be determined and updated along with the rest of the fields in the fine-grid region. In previous sub-gridding techniques [1]–[3], the wave equation was used to update these field values. However, even if losses are accounted for in the wave equation, these techniques become unstable when traversing material boundaries. Others have used interpolation of the coarse magnetic field to provide the fine-region magnetic fields that are necessary for using the traditional FDTD equations [5]. By using interpolated magnetic fields and the standard update equations for the electric fields on the interface boundary, it becomes possible to traverse dielectric boundaries. Although the technique presented here also uses the coarse-grid magnetic fields and the traditional FDTD equations, thus allowing for material traverse, it does not use interpolation. Instead, the current passing through the surface enclosed by the coarse-region contour ($\oint H \cdot d\ell$) is scaled according to the material properties and the area of the fine-region contour to provide the current values necessary in the calculation of the electric-field update equations. Since the technique presented here uses the current from the coarse grid to update the tangential-field values on the interface boundary, this technique is henceforth referred to as the multigrid current method (MGCM). The uniqueness of this technique is that it enables the solution of the multigrid problem while maintaining the integrity of the standard FDTD equations. Also, unlike the technique describe in [5], this technique will work for any integer refinement factor. It remains stable for a Courant number of 0.57. The procedure to be described is simple to program and results in improved resolution in regions of interest. Having the capabilities to traverse dielectric boundaries makes this technique applicable to a wide variety of problems where increased resolution is required, but previously unattainable.

III. Solution Procedure

To show how the tangential electric fields on the interface boundary are updated, we start with Ampere's law in integral form

$$\oint_c H \cdot d\ell = \int_S \sigma E \cdot dS + \frac{d}{dt}\int_S \varepsilon E \cdot dS. \tag{2}$$

Fig. 1 shows a two-dimensional view of the electric and magnetic fields at the interface boundary using the standard Yee cell.

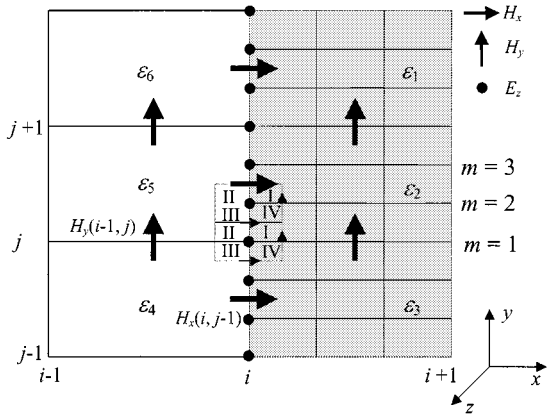

Fig. 1. Schematic illustration of the magnetic fields of the coarse- and fine-grid contours defining the electric current at the interface boundary. This figure shows a mesh refinement ($n\text{fact}$) of three. The coarse-grid region is located on the left-hand side, while the fine-grid region is shaded on the right-hand side.

The left-hand side of (2), the total current passing through the surface of the coarse-grid contour I_{Tc} can be written as

$$I_{Tc} = \oint_c H \cdot d\ell = \Big[H_x(i, j-1) + H_y(i, j) - H_x(i, j) - H_y(i-1, j)\Big]\Delta\ell_c. \tag{3}$$

The right-hand side of (2) can be solved by calculating the contribution of each media type to the integral, thus,

$$\begin{aligned}\int_S \sigma E \cdot dS + \frac{d}{dt}\int_S \varepsilon E \cdot dS &= \int_S \left(\sigma_2 E_z + \frac{d}{dt}\varepsilon_2 E_z\right) dS_{\varepsilon_2} \\ &+ \int_S \left(\sigma_3 E_z + \frac{d}{dt}\varepsilon_3 E_z\right) dS_{\varepsilon_3} \\ &+ \int_S \left(\sigma_4 E_z + \frac{d}{dt}\varepsilon_4 E_z\right) dS_{\varepsilon_4} \\ &+ \int_S \left(\sigma_5 E_z + \frac{d}{dt}\varepsilon_5 E_z\right) dS_{\varepsilon_5}.\end{aligned} \tag{4}$$

The total current can subsequently be broken into parts according to the dielectric material

$$I_{Tc} = I_{\varepsilon_2} + I_{\varepsilon_3} + I_{\varepsilon_4} + I_{\varepsilon_5} \tag{5}$$

where, e.g.,

$$\begin{aligned} I_{\varepsilon_2} &= \Big[(1+\overline{\sigma_2})E_z^{n+1} - (1-\overline{\sigma_2})E_z^n\Big]\frac{\varepsilon_0\varepsilon_{r2}\left(\frac{\Delta\ell_c}{2}\right)^2}{\Delta t_c} \\ \overline{\sigma_2} &= \frac{\sigma_2\Delta t_c}{2\varepsilon_0\varepsilon_{r2}}. \end{aligned} \tag{6}$$

Using this notation, the standard FDTD update equation can be written as

$$\begin{aligned} E_z^{n+1} &= \left(\frac{1-\overline{\sigma}_c}{1+\overline{\sigma}_c}\right)E_z^n + \frac{C_n\eta_0}{\langle\varepsilon_0\rangle(1+\overline{\sigma}_c)}\frac{I_{Tc}}{\Delta\ell} \\ \overline{\sigma}_c &= \frac{1}{2}\frac{0.25*(\sigma_2+\sigma_3+\sigma_4+\sigma_5)}{0.25*(\varepsilon_{r2}+\varepsilon_{r3}+\varepsilon_{r4}+\varepsilon_{r5})} = \frac{\langle\sigma\rangle\Delta t}{2\langle\varepsilon_r\rangle\varepsilon_0} \\ C_n &= \text{Courant Stability Number} = \frac{c\Delta t_c}{\Delta\ell_c} \end{aligned} \tag{7}$$

where I_{Tc} is obtained from (3). A similar FDTD update equation can be written for the fine region. However, since the cur-

rent passing through the surface defined by the fine-region contour (I_{Tf}) at the interface boundary is not known, it must be determined using the current passing through the coarse-region surface. This may be done by calculating the fraction of current passing through the coarse-region surface that also passes through the fine-region surface. By assuming that the total current is not changing during the $n\text{fact}$ iterations of the fine region, even though the individual magnetic fields in the fine region are, the standard update equations can be applied.

To calculate the current passing through the fine-region surface, we note that this surface also has four possible media types. The four quadrants of the contour surrounding the fine-region electric field (Fig. 1) each contribute to the integral. Thus,

$$I_{Tf} = I_{\text{I}} + I_{\text{II}} + I_{\text{III}} + I_{\text{IV}}. \tag{8}$$

Referring to Fig. 1, for the calculation of the tangential electric field located at $m = 1$, quadrants I–IV are located in regions ε_2, ε_5, ε_4, and ε_3, respectively. For the calculation of the electric field located at $m = 2$, quadrants I and IV are located in ε_2, while quadrants II and III are located in ε_5. To calculate individual currents passing through the fine surface, the individual currents passing through the coarse surface are multiplied by a scale factor. This scale factor is simply the ratio of the respective areas. Thus, the current used to update the fine-region tangential field at $m = 1$ is given by

$$\begin{aligned} I_{Tf} &= I_{\text{I}} + I_{\text{II}} + I_{\text{III}} + I_{\text{IV}} \\ &= \left(I_{\varepsilon_2} + I_{\varepsilon_5} + I_{\varepsilon_4} + I_{\varepsilon_3}\right)\frac{\Delta\ell_f^2}{\Delta\ell_c^2} \\ &= \frac{I_{Tc}}{n\text{fact}^2}. \end{aligned} \tag{9}$$

Since the current passing through the coarse-grid surface [see (3)] is known when the iteration in the fine region begins, this calculation is straight forward. However, when the fine-region tangential field is not at the center of the coarse-region contour, i.e., $m \neq 1$, some approximations must be made. Following a similar procedure, the current used for updating the fine-region tangential electric field at $m = 2$ can be written as

$$I_{Tf} = \left(I_{\varepsilon_2} + I_{\varepsilon_5} + I_{\varepsilon_5} + I_{\varepsilon_2}\right)\frac{1}{n\text{fact}^2}. \tag{10}$$

The individual components can be calculated as fractions of the total current by using (6) and (7) as follows:

$$\frac{I_{\varepsilon 2}}{I_{Tc}} = \frac{\left[\left(1+\overline{\sigma_2}\right)E_z^{n+1} - \left(1-\overline{\sigma_2}\right)E_z^n\right]}{\left[\left(1+\overline{\sigma_c}\right)E_z^{n+1} - \left(1-\overline{\sigma_c}\right)E_z^n\right]}\frac{\frac{\varepsilon_2}{4}}{\varepsilon_c}. \tag{11}$$

Therefore, (10) can be written as

$$I_{Tf} = \frac{\left[\left(1+\overline{\sigma_{fc}}\right)E_z^{n+1} - \left(1-\overline{\sigma_{fc}}\right)E_z^n\right]}{\left[\left(1+\overline{\sigma_c}\right)E_z^{n+1} - \left(1-\overline{\sigma_c}\right)E_z^n\right]}\frac{\varepsilon_f}{\varepsilon_c}\frac{I_{Tc}}{n\text{fact}^2} \tag{12}$$

where

$$\begin{aligned} \varepsilon_f &= (2\varepsilon_2 + 2\varepsilon_5) \\ \overline{\sigma_{fc}} &= (2\sigma_2 + 2\sigma_5)\frac{\Delta t_c}{2\varepsilon_f\varepsilon_0} \\ \varepsilon_c &= (\varepsilon_2 + \varepsilon_5 + \varepsilon_4 + \varepsilon_3) \\ \overline{\sigma_c} &= (\sigma_2 + \sigma_5 + \sigma_4 + \sigma_3)\frac{\Delta t_c}{2\varepsilon_c\varepsilon_0}. \end{aligned} \tag{13}$$

Equation (12), when programmed, can be used to update the tangential fields at the interface boundary. However, this equation can be further simplified given either of the following conditions:

$$\overline{\sigma_c} = \overline{\sigma_{fc}}$$

or

$$\overline{\sigma_c} \ll 1 \text{ and } \overline{\sigma_{fc}} \ll 1. \tag{14}$$

For either of the special cases in (14), (12) can be written as

$$I_{Tf} = I_{Tc}\frac{\varepsilon_f}{\varepsilon_c}\frac{1}{n\text{fact}^2} = \delta_f I_{Tc}. \tag{15}$$

Using (15), the standard FDTD update equation for the tangential fields on the boundary can be written in the following form:

$$E_z^{n_f+1} = \left(\frac{1-\overline{\sigma}_f}{1+\overline{\sigma}_f}\right)E_z^{n_f} + \frac{Cn\eta_0}{(0.25\varepsilon_f)(1+\overline{\sigma}_f)}\frac{1}{\Delta\ell_f}\delta_f I_{Tc}. \tag{16}$$

Equation (16) represents the general form of the interface-boundary update equation which, along with (3), forms the basis of the developed sub-gridding technique (i.e., MGCM).

The limits of this technique are given by (14). The first of the conditions is valid for all cases when the current contour does not traverse any dielectric boundaries. Therefore, in all simulations where the interface boundary does not traverse any dielectric boundary, the formulation is valid. The second limiting condition applies when traversing dielectric boundaries. It can be shown that this limiting condition holds if the loss tangent of the boundary material is much less than the number of time steps per cycle (N_t) divided by π, i.e.,

$$\frac{\langle\varepsilon''\rangle}{\langle\varepsilon'\rangle} \ll \frac{N_t}{\pi}$$

or

$$\frac{\langle\varepsilon''\rangle}{\langle\varepsilon'\rangle} \ll 8, \qquad \text{for } N_t = 25. \tag{17}$$

In our simulations of microwave sintering and RF drying [6]–[8], the material with the highest loss tangent is SiC, with a loss tangent of 0.23 at 2.45 GHz. Although this is a high loss tangent, it still meets the criteria set by (17). Therefore, this technique is applicable to a wide variety of numerical modeling projects.

When neither of the two conditions in (14) are met, the effect is to create a "soft" boundary between materials. The location where one media ends and another begins is no longer a distinct plane. Instead, the dielectric properties of the two media types are averaged over $n\text{fact}$ fine-grid cells (one coarse grid cell), creating the "soft" transition region. To avoid this problem, it is possible to program (12) or increase the size of the fine-grid region so that it encloses the entire medium whose loss tangent is greater than the allowed values. However, it will be shown later that the "soft" transition region still provides an accurate overall simulation of a large fine region. This results in a sub-gridding program that is very powerful and simple to use for traversing almost any media boundary subject to satisfying (17), and this includes the case of perfect electric conductors (PECs).

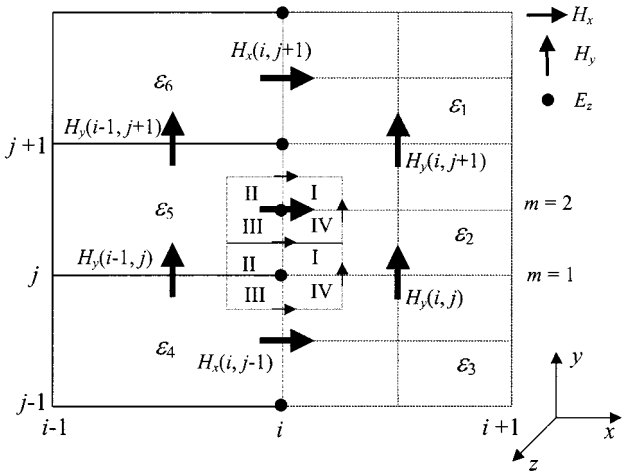

Fig. 2. Schematic illustrating the magnetic fields of the coarse- and fine-grid regions at the interface boundary when the integer refinement factor is even. When $m = 2$, the electric field is located between the current contour centers at (i, j) and $(i, j+1)$. Therefore, the current passing through the fine-grid surface at $m = 2$ is calculated based on the average of the two coarse-grid current contours [i.e., the currents centered at (i, j) and $(i, j+1)$].

IV. General Formulation

There are five values of the fine-grid reference number m that must be considered in order to provide a general formulation. These include $m = 1$, $m < \text{half}$ ($\text{half} = n\text{fact}/2 + 1$), $m = \text{half}$ when $n\text{fact}$ is odd, $m = \text{half}$ when $n\text{fact}$ is even, and $m > \text{half}$. The first two cases have previously been described. It can be readily shown that when $n\text{fact}$ is odd and $m = \text{half}$, the equations are the same as when $m < \text{half}$. Fig. 2 shows the special case when the integer refinement factor is even and the update calculation is for the field co-located with the coarse-region magnetic field $(m = 2)$. In this case, the total current is calculated by using six magnetic fields, which may pass through six different media types. From Fig. 2, the total coarse-region current is calculated as

$$I_{Tc} = \oint_c H \cdot d\ell = \Big[H_x(i, j-1) + H_y(i, j) + H_y(i, j+1) - H_x(i, j+1) - H_y(i-1, j+1) - H_y(i-1, j)\Big]\Delta\ell_c. \tag{18}$$

Following the procedure outlined above, and taking into account the six current contributors from the coarse-region contour, it can be shown that the scale factor for this case is given by

$$\delta_f = \frac{(2\varepsilon_2 + 2\varepsilon_5)}{(\varepsilon_1 + 2\varepsilon_2 + \varepsilon_3 + \varepsilon_4 + 2\varepsilon_5 + \varepsilon_6)} \frac{1}{n\text{fact}^2}. \tag{19}$$

For the final condition, when $m > \text{half}$, it may be shown that the current contour is centered at $(i, j+1, k)$ instead of (i, j, k), as is done for $m < \text{half}$. This also results in using different media references (i.e., media type 3 in (13) is replaced with media type 1, and media type 4 in (13) is replaced with media type 6). Now that the five possibilities for the reference number m have been described, the scale factor can be written as (20), shown at the bottom of this page, where "m" is the index of the fine-region field and is limited to $1 \leq_m \leq n\text{fact}$. Since the scale factor contains no time dependence, it can be calculated before starting the iteration process, and the resulting values can be included in the constants used to update the interface-boundary electric fields.

Therefore, in order to sub-grid the FDTD technique using the MGCM, we assume that the total current passing through the surface bounded by the FDTD contour is not changing while the fine region is being updated. The current from the coarse region, after being scaled appropriately, can then be used in the update equations for the tangential electric fields on the boundary. This results in an electric-field update equation on the boundary that is similar to the update equations for the fields inside of the fine-grid region.

Once the fine-grid region is updated $n\text{fact}$ times, the final step of updating the coarse region with the values from the fine-grid region is performed. The method that provides the most stability and accuracy is described in [1]. Although the sub-gridding technique is different here, the method for updating the coarse region is still the most stable and accurate. Updating the coarse region proceeds as follows: the coarse-grid electric fields that lie on the first cell inside the fine region (the interface boundary cells) are left unchanged, the coarse-grid electric fields that lie on the second cell inside the fine region are replaced by the average of the values from the fine- and coarse-grid regions, and coarse-grid cells that are more than two cells within the fine-grid region are replaced by the value obtained in the fine-grid region. The result is a two-coarse-cell overlapping region that improves the stability of the solution.

$$\delta_f = \begin{cases} \dfrac{1}{n\text{fact}^2}, & m = 1 \\ \dfrac{(2\varepsilon_2 + 2\varepsilon_5)}{\varepsilon_2 + \varepsilon_3 + \varepsilon_4 + \varepsilon_5} \dfrac{1}{n\text{fact}^2}, & m < \text{half} \\ \dfrac{(2\varepsilon_2 + 2\varepsilon_5)}{\varepsilon_2 + \varepsilon_3 + \varepsilon_4 + \varepsilon_5} \dfrac{1}{n\text{fact}^2}, & m = \text{half and } n\text{fact odd} \\ \dfrac{(2\varepsilon_2 + 2\varepsilon_5)}{\varepsilon_1 + 2\varepsilon_2 + \varepsilon_3 + \varepsilon_4 + 2\varepsilon_5 + \varepsilon_6} \dfrac{1}{n\text{fact}^2}, & m = \text{half and } n\text{fact even} \\ \dfrac{(2\varepsilon_2 + 2\varepsilon_5)}{\varepsilon_2 + \varepsilon_1 + \varepsilon_5 + \varepsilon_6} \dfrac{1}{n\text{fact}^2}, & m \geq \text{ half} \end{cases} \tag{20}$$

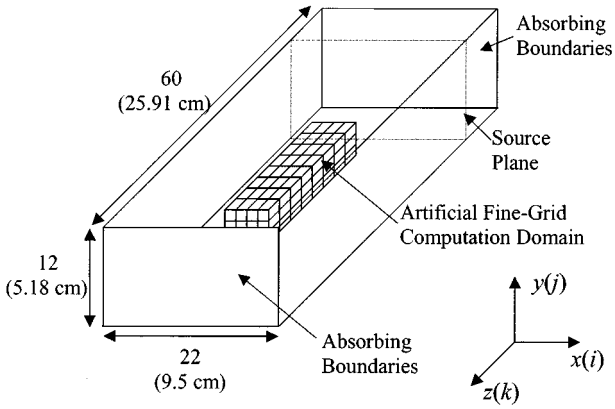

Fig. 3. Schematic illustration of the waveguide used in evaluating the accuracy of the MGCM solution procedure. Dimensions are given in node numbers and centimeters. To evaluate the accuracy of the MGCM procedure, an artificial fine-grid computation domain was placed in the WR340 air-filled waveguide. The reflection coefficient due to the artificial domain, as well as magnitude and phase errors at the center of the fine-grid region, were calculated.

V. Stability and Accuracy of the Developed MGCM Technique

In this section, we will present two examples that illustrate the improved stability and accuracy of the developed technique, and a simulation illustrating the application of the MGCM to a model that was previously impossible to simulate.

A. Simulation of Artificial Fine-Grid Region in an Air-Filled Waveguide

To evaluate stability and accuracy of the new FDTD code, an air-filled waveguide (WR 340) was modeled and simulated at 2.45 GHz. Magnitude and phase errors at the center of the fine region were calculated when a TE_{10} mode was launched in the waveguide. Fig. 3 shows the waveguide and simulation parameters. For comparison, results from the MGDM [1] code developed by our group are presented along with the new MGCM simulation results. In [1], it was shown that the MGDM is more stable and more accurate than other methods such as the VSSM [2] method, especially when modeling complex and/or large structures inside the fine region. Therefore, calculations based on the VSSM method are not presented here. Fig. 4 shows the magnitude and phase errors at the center of the fine region and the reflection coefficient introduced by the multigrid boundary when the refinement factor $n\mathrm{fact}$ is varied from 2 to 11. Since some errors are introduced by FDTD (errors due to dispersion and absorbing boundaries, etc.), for accuracy purposes, the results of the multigrid simulations are compared to results from a uniform-grid simulation with resolution equal to that of the fine regions of the multigrid codes. The reflection coefficient and magnitude and phase errors were calculated as follows:

$$\Gamma(\text{center of waveguide}) = \frac{E_y^-}{E_y^+} \tag{21}$$

$$e_{\mathrm{MAG}} = \left| \frac{E_{\mathrm{uniform}} - E_{mg}}{E_{\mathrm{uniform}}} \right| \tag{22}$$

$$e_{\mathrm{phase}} = \left| \frac{\Delta t}{T} \right| \times 360^\circ. \tag{23}$$

As may be seen from Fig. 4, the new sub-gridding formulation is much more accurate, even when the boundary between the fine and coarse grid contains no dielectric boundaries. The observed reflection coefficient value of 1% may also include contributions from the absorbing boundary conditions and, hence, the accuracy of MGCM may be better than the reported 1%. Although it is not shown, it was found that the long-term stability of the MGCM is also improved over that of the MGDM. No signs of numerical instability were noticed even when the running time was in excess of 20 cycles.

B. Simulation of Fields in a Waveguide Containing a Dielectric Region or a PEC

The most important aspect of this new sub-gridding technique is the ability to traverse media boundaries. Therefore, simulations were made in a WR340 waveguide containing a dielectric sample. The size of the dielectric sample was $12 \times 4 \times 12$ coarse cells or $51.8 \times 13.0 \times 51.8$ cm^3. The fine-grid region had dimension of $16 \times 6 \times 8$ coarse cells. Fig. 5 shows a drawing of the model used in the simulations. Two different simulations were made to evaluate the effect of the loss tangent on simulation accuracy. The two material properties simulated were $\varepsilon = (10 + j1)_{\varepsilon_0}$ and $\varepsilon = (10 + j10)_{\varepsilon_0}$, corresponding to loss tangents of 0.1 and 1.0, respectively. For these simulations, a mesh-refinement factor of $n\mathrm{fact} = 3$ was chosen. Once again, a uniform-grid FDTD code with the same resolution as the fine grid of the multigrid FDTD code was used for comparison. In Fig. 6, magnitude-error mesh plots of the dominant E_y fields are shown for a horizontal slice (constant y). The percentage errors were calculated using (21). As can be seen in Fig. 6(a), when the loss tangent is only 0.1, the developed technique provides very accurate results. In fact, the average error, calculated over the entire slice, is approximately 2%. Fig. 6(b) shows the same slice when the material properties are changed to the case of a loss tangent of 1.0. This, of course, violates the approximation given in (14). The results in Fig. 6(b), however, show that poor values were obtained only at the location of the media interface. As expected, the result of the approximation was to create a soft transition region in which the effective loss tangent at that boundary was smaller than the actual loss tangent, thus creating errors. However, throughout the rest of the fine-grid region, the errors remained small. The average error over the entire slice for this simulation was approximately 4%, which is still certainly acceptable.

Another example to show the capability of traversing dielectrics is the calculation of the resonant frequency of a rectangular resonator with a dielectric load [9]. The cavity has dimensions of $24 \times 12 \times 16$ mm and a dielectric load with a thickness of 8 mm and a relative dielectric constant of 3.75 (see Fig. 7). Three cases are calculated. In the first case, a coarse uniform grid with mesh size of 4.0 mm is used. In the second case, a fine grid with mesh size of 1.0 mm is employed. In the third case, we use the multigrid with the coarse mesh size 4.0 mm and the fine mesh size 1.0 mm ($n\mathrm{fact} = 4$). The fine grid has dimensions of $8 \times 4 \times 8$ mm with two faces traversing the dielectric (see Fig. 7). The resonant frequency of the fundamental mode is compared with the results of transmission-line matrix (TLM) and FDTD of [9] in Table I. It can be seen that

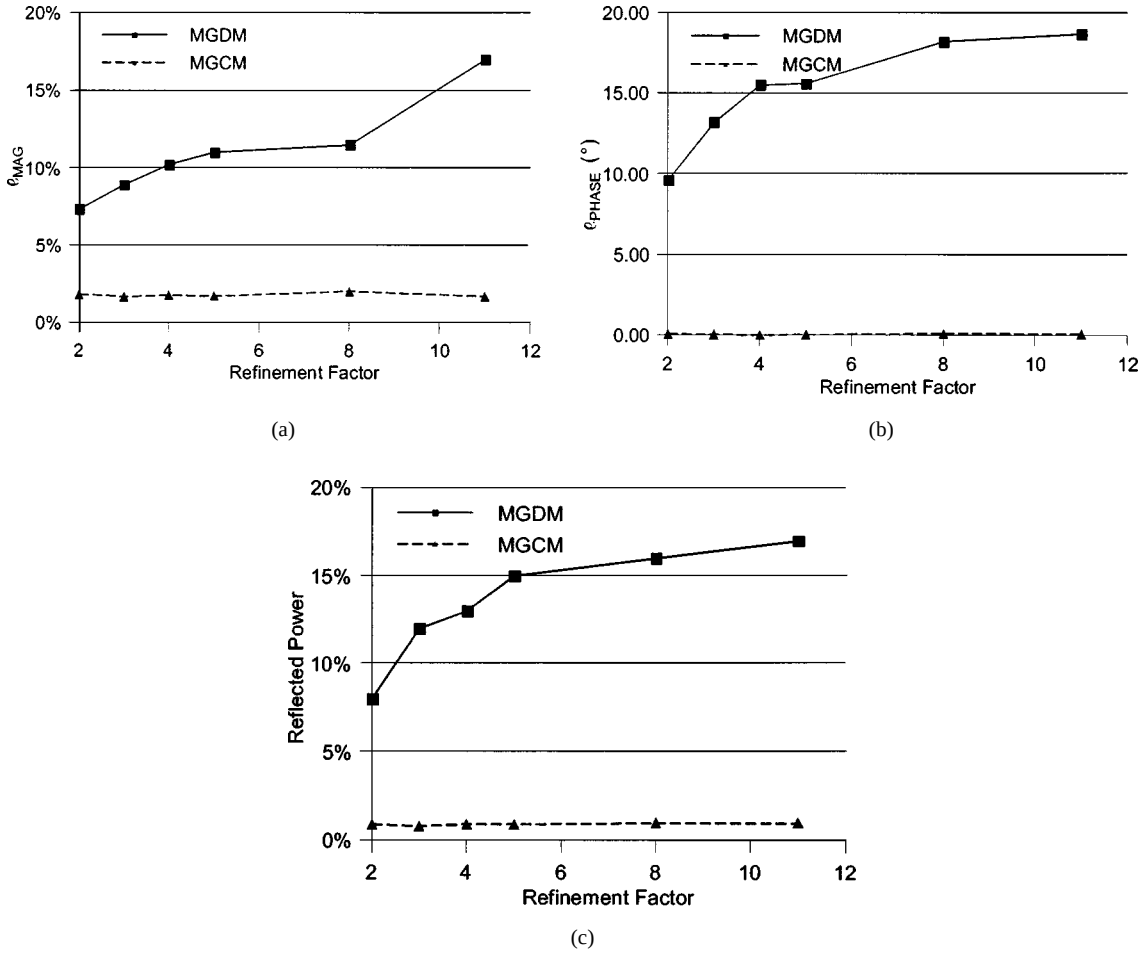

Fig. 4. Comparison of the accuracy of the MGDM and MGCM sub-gridding techniques when an artificial fine-grid region is placed in an air-filled waveguide. Calculations for the: (a) magnitude (e_{MAG}) errors and (b) phase (e_{PHASE}) errors were made at the center of the fine-grid region while the (c) reflection coefficient was calculated at the center of the waveguide, two cells behind the location of the source launch.

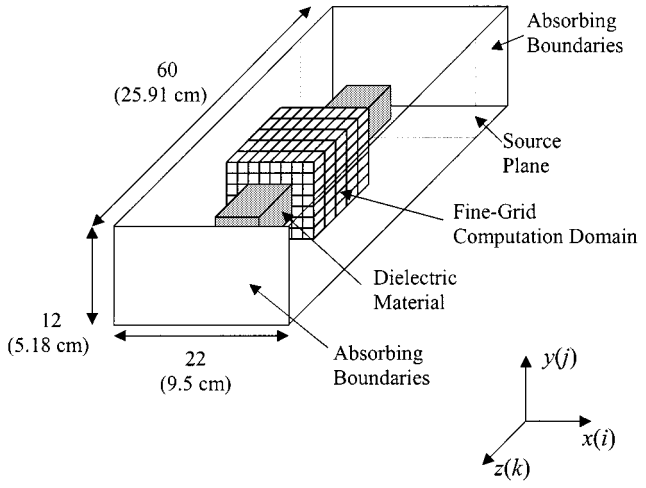

Fig. 5. Schematic illustration of the WR340 waveguide, dielectric material, and artificial fine-grid computation domain that was used to evaluate the accuracy of traversing a dielectric boundary. Dielectric materials of two different loss tangents (0.1 and 1.0) were simulated.

the multigrid method can improve the accuracy of solution with a modest increase in the computational resources.

In addition to traversing dielectric boundaries, the MGCM interface boundary can traverse perfect conductors. To demonstrate this flexibility, two simulations in the same WR340 waveguide were performed. The first simulation used the same simulation parameters as the dielectric-traverse simulations just discussed. However, the dielectric material was given the properties of a perfect conductor. Therefore, a fine-grid region of dimensions $16 \times 6 \times 8$ was centered around a perfect conductor with dimensions of $12 \times 4 \times 12$. In the second simulation, the fine-grid region was lengthened so that it was the same length as the perfect conductor, resulting in fine-grid dimensions of $16 \times 6 \times 12$. This simulation placed two faces of the fine grid at the faces of the perfect conductor. Eight simulation cycles were calculated using these two arrangements and a uniform-grid FDTD code. The reflected waves were then compared at each time step in the eight simulation cycles. Fig. 8 shows the three reflected waves. The "outside" wave corresponds to the case when the perfect conductor extends outside the fine-grid region at the multigrid interface boundaries. Note that no special treatment of the perfect conductor was needed for these simulations. The ability of MGCM to allow perfect conductors to traverse the interface boundary results from using standard FDTD update equations that automatically account for PECs.

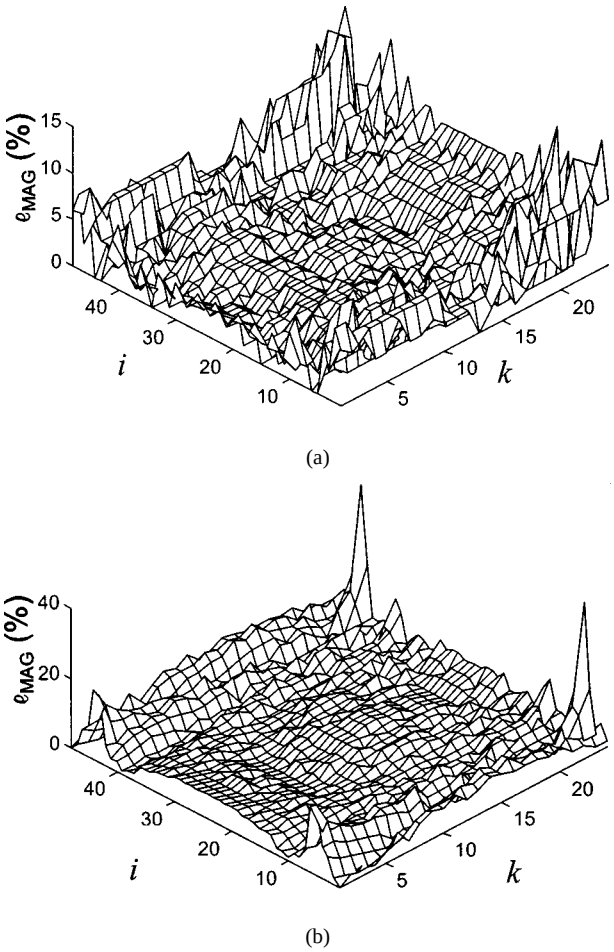

Fig. 6. Horizontal slice through the center of the fine-grid region of the waveguide simulation that contained dielectric material. The electric-field magnitude percent errors (e_{MAG}) were calculated. Results of dielectric materials with a relatively low loss tangent of: (a) 0.1 and a relatively high loss tangent of (b) 1.0 were simulated. It should be noted that large errors at $k = 24$ (back edge in the pictures) represent errors from relatively small electric-field values. Simulation results show that the electric-field values at these edges are almost an order of magnitude lower than those in the middle.

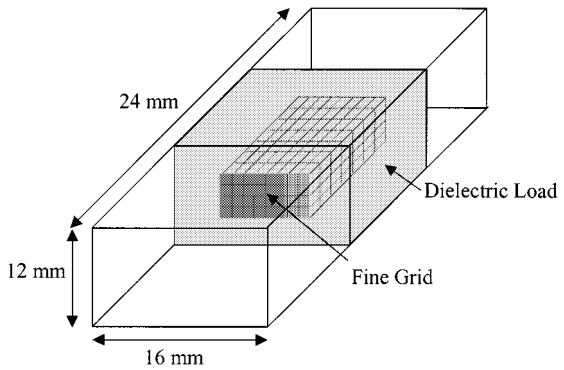

Fig. 7. Rectangular resonator with dimensions 16 × 12 × 24 mm. The dielectric load has dimensions of 16 × 12 × 8 mm and a relative dielectric constant 3.75. The fine grid area is also shown.

C. Simulation of Microwave Processing in Large Multimode Cavities

The MGCM was developed to facilitate simulation of electrically large and complex structures, which could not be simulated previously due to excessive memory requirements. To illustrate the numerical advantages of the new MGCM technique, a simulation of ceramic sintering in a large (500 L) multimode microwave cavity that contained multiple layers of bucket tappet samples with wall thickness of 0.32 cm (0.03 λ) was performed. Since the frequency of operation was 2.45 GHz ($\lambda = 12.2$ cm), the wavelength is 38 times the sample thickness and 76 times the minimum required resolution. The coarse grid was modeled using a 1.17-cm cell size and the fine grid used a 0.146-cm cell size (reduction factor of eight). The microwave cavity was cylindrical with a diameter of 74 cm (6 λ) and length of 112 cm (9 λ). Dimensions of the coarse and fine grid regions were 63 × 63 × 113 cells and 144 × 136 × 144 cells, respectively. Four layers, each containing a 3 × 3 array of bucket tappet samples, were modeled. The dielectric properties of the sample were $\varepsilon_r = 7.40$ and $\sigma = 0.02$ S/m and the sample height was 1.0 cm. The sample had a square cross section of 2 × 2 cm^2 and a wall thickness of 0.33 cm. Alumina shelves with dielectric properties of $\varepsilon_r = 3.36$ and $\sigma = 0.0017$ S/m supported the four layers of samples. The simulated cavity model represents a realistic microwave sintering experiment and also includes a boron–nitride (BN) crucible box with dielectric properties of $\varepsilon_r = 3.45$ and $\sigma = 0.00045$ S/m and an alumina-fiberboard box with dielectric properties of $\varepsilon_r = 1.52$ and $\sigma = 0.00019$ S/m, which encloses the entire sintering arrangement. Results of electric-field

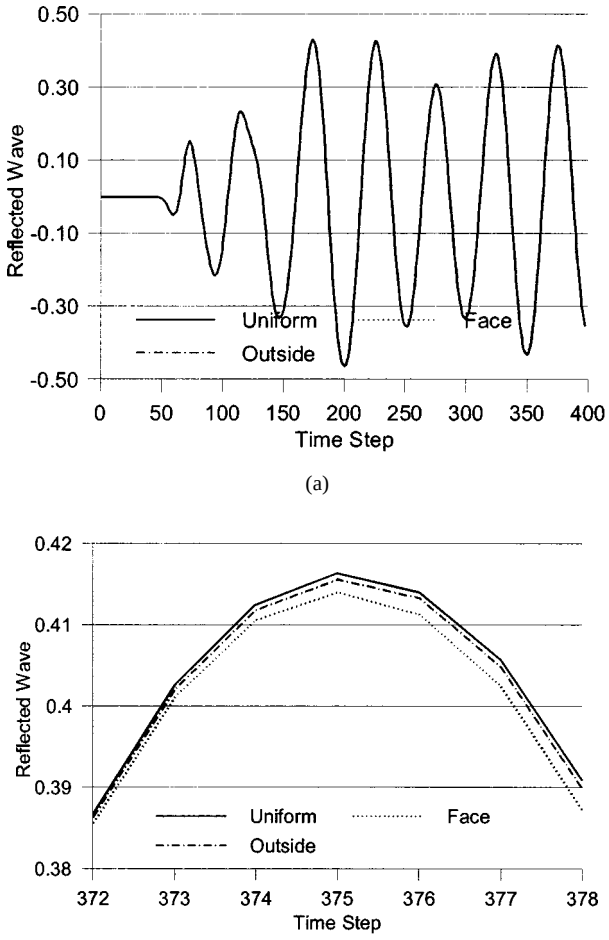

Fig. 8. Transient plot of the reflected wave when the MGCM interface boundary traversed a perfect conductor. (a) Full eight cycle simulation. (b) Blown-up portion of the final cycle.

TABLE I
RESONANT FREQUENCIES OF THE INHOMOGENIOUS RESONATOR

Method	Resonant Frequency (GHz)	Difference with TLM (%)	Difference with FDTD (%)
TLM [9]*	6.60	-	-
FDTD [9]*	6.63	-	-
Coarse uniform mesh	6.71	1.67	1.21
Fine uniform mesh	6.66	0.91	0.45
Multigrid	6.63	0.45	0.0

* The resonant frequencies in [9] are normalized as $\Delta l / \lambda$. To obtain unnormalized values, we have chosen $\Delta l = 2$ mm and the values in this table are converted from the normalized values in [9].

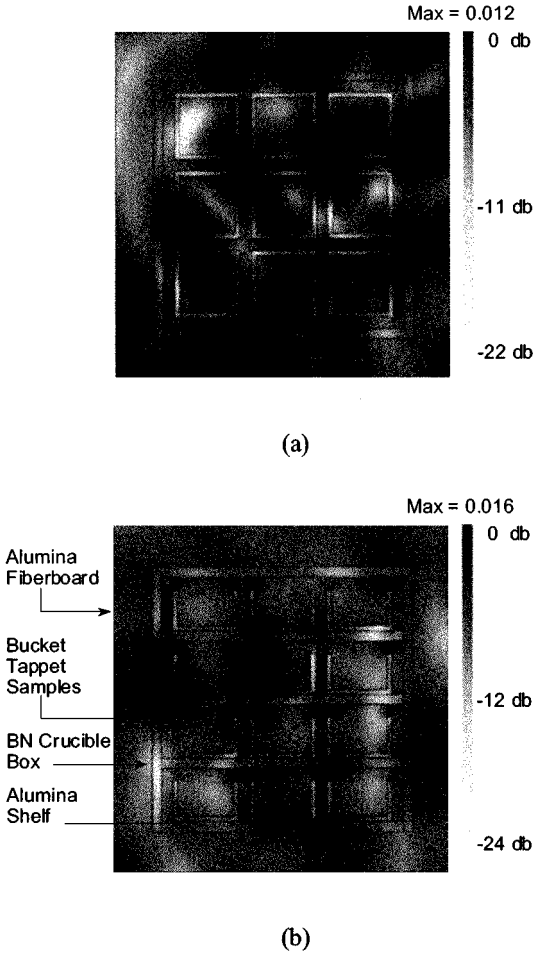

Fig. 9. Electric field ($|E|^2$) distribution patterns in the fine-grid region of an MGCM simulation of a large-scale 500-L multimode microwave cavity. (a) Horizontal cross section showing a j = constant plane. (b) Vertical cross section showing a k = constant plane. The MGCM is the only method currently capable of simulating this cavity using the required resolution enforced by the sample size used in these experiments.

patterns in the cavity modeled by the fine region are shown in Fig. 9. If a uniform grid code had been used to model the entire multimode cavity with a resolution of 0.146 cm (the same as the fine-grid region of the MGCM code), the memory required would have increased by a factor of 70, which would have prohibited the simulation of such a structure.

VI. SUMMARY AND CONCLUSIONS

In this paper, we have described a new technique for sub-gridding the FDTD method. It is simple, accurate, and, most importantly, can be used for any $n\mathrm{fact}$. We simulated cases for $n\mathrm{fact}$ up to 11. The ability to use a Courant number close to its maximum value of 0.57 with different values of $n\mathrm{fact}$ and the ability to traverse dielectric and PEC boundaries shows clear improvement and advances as compared with other available techniques. The solution procedure is based on using weighted values of the electrical current to make the transition from the coarse- to fine-grid regions. The fine-grid current values are then used to determine the field values in the fine-grid region. Both the material properties and relative position of the fine-grid electric field within the current contour are used in determining the weighting function. Simulations were performed to evaluate the stability and accuracy of the new technique. It was determined that the introduction of a high-resolution sub-grid region in an FDTD code introduced only a slight reflection in the larger, coarse-grid region (2% reflection). This additional high-resolution sub-grid region provides accurate simulation results in areas of interest when memory prohibits the use of a uniform FDTD code. In addition, this technique allows for material traverse without reducing the Courant number in order to maintain stability, and the developed method is also general enough to allow for any integer refinement factor. The equations that need to be programmed are simple and maintain the basic form of the standard FDTD update equations. The development of this sub-gridding technique allows for modeling complex structures in large models where it was previously impossible to increase the resolution. For example, a microwave sintering experiment in which the new technique was used required 2 h 45 min for a 173-MB executable program. If the same resolution had been used in a uniform-grid code, the executable would have been over 12 GB, and would have required approximately 225 h to execute. The developed MGCM code resulted in a 70× reduction in memory and a 80× reduction in execution time. This simulation also contained a conveyor belt, which made it impossible to use other available sub-gridding techniques that did not allow traversing dielectric boundaries. Even simulations that may have been performed using a uniform-grid code can now be optimized for speed and accuracy using the new technique. We are currently applying this new technique to research projects in

the areas of microwave processing of materials, high-frequency modeling of electronic packages, and bioelectromagnetics. The developed method allows for unprecedented resolution while maximizing the use of available computational resources.

REFERENCES

[1] M. J White, M. F. Iskander, and Z. Huang, "Development of a multi-grid FDTD code for three-dimensional applications," *IEEE Trans. Antennas Propagat.*, vol. 45, pp. 1512–1517, Oct. 1997.

[2] S. S. Zivanovic, K. S. Yee, and K. K. Mei, "A subgridding method for the time-domain finite-difference method to solve Maxwell's equations," *IEEE Trans. Microwave Theory Tech.*, vol. 39, pp. 471–479, Mar. 1991.

[3] D. T. Prescott and N. V. Shuley, "A method for incorporating difference sized cells into the finite-difference time-domain analysis technique," *IEEE Microwave Guided Wave Lett.*, vol. 2, pp. 434–436, Nov. 1992.

[4] M. Okoniewski, E. Okoniewska, and M. A. Stuchly, "Three-dimensional subgridding algorithm for FDTD," *IEEE Trans. Antennas Propagat.*, vol. 45, pp. 422–429, Mar. 1997.

[5] M. W. Chevalier, R. J. Luebbers, and V. P. Cable, "FDTD local grid with material traverse," *IEEE Trans. Antennas Propagat.*, vol. 45, pp. 411–421, Mar. 1997.

[6] M. J. White, S. F. Dillon, M. F. Iskander, and H. D. Kimrey, "FDTD simulation of microwave sintering in a variable frequency multimode cavity," in *Proc. Mater. Res. Soc. Symp. Dig.*, vol. 430, Microwave Process. Mater. V, San Francisco, CA, Apr. 1996, pp. 487–492.

[7] M. Subirats, M. F. Iskander, and M. J. White, "FDTD simulation of microwave sintering in large (500/4000 liter) multimode cavities," in *Proc. Mater. Res. Soc. Symp. Dig.*, vol. 430, Microwave Process. Mater. V, San Francisco, CA, Apr. 1996, pp. 29–36.

[8] S. Bringhurst, M. J. White, and M. F. Iskander, "Validation of FDTD simulation results using an experimental RF dryer," in *Proc. Mater. Res. Soc. Symp. Dig.*, vol. 430, Microwave Process. Mater. V, San Francisco, CA, Apr. 1996, pp. 487–492.

[9] D. H. Choi and W. J. R. Hoefer, "The finite-difference time-domain method and its application to eigenvalue problems," *IEEE Trans. Microwave Theory Tech.*, vol. MTT-34, pp. 1464–1469, Dec. 1986..

Mikel J. White (S'95–M'97), photograph and biography not available at time of publication.

Zhengqing Yun (M'98) received the Ph.D. degree in electrical engineering from Chongqing University, Chongqing, China, in 1994.

From 1995 to 1997, he was a Post-Doctoral Fellow in the State Key Laboratory of Millimeter Wave, Southeast University, Nanjing, China. Since 1997, he has been with the Electrical Engineering Department, University of Utah, Salt Lake City, where he is currently a Research Assistant Professor. His current research interests include development of numerical methods and modeling of radio propagation for wireless communications systems.

Dr. Yun was the recipient of the 1997 Science and Technology Progress Award (First Class) presented by The State Education Commission of China.

Magdy F. Iskander (S'72–M'76–F'93) is currently a Professor of electrical engineering at the University of Utah, Salt Lake City. From 1997 to 1999, he was the Program Director, Physical Foundation of Enabling Technologies, in the Electrical and Communication Systems Division, National Science Foundation (NSF), where he formulated and directed a "Wireless Technologies and Information Networks" initiative in the Engineering Directorate. This wireless communications initiative resulted in the funding of over 29 projects in the microwave/millimeter-wave devices, propagation, and antennas areas. He has been with the University of Utah since 1977, and is currently the Director of the Center of Excellence for Multimedia Education and Technology (formerly the NSF/IEEE Center for Electromagnetics Education). In 1986, he established the Engineering Clinic Program to attract industrial support for projects to be performed by engineering students at the University of Utah. Since then, over 95 projects have been sponsored by 29 corporations from across the U.S. The Clinic Program now has a large endowment for scholarships and a professorial chair. From 1994 to 1997, he was the Director of the Conceptual Learning of Science (CoLoS) USA Consortium, which is sponsored by the Hewlett-Packard Company and has 11 member universities from across the U.S. He spent sabbatical leaves at the Polytechnic University of New York, Ecole Superieure D'Electricite, University of California at Los Angeles, Harvey Mudd College, Tokyo Institute of Technology, Polytechnic University of Catalanya, and several universities in China, including Tsinghua University, South East University, Shanghai Jiaotong University, Suzhou University, and Yangzhou University. He has authored or co-authored over 160 papers in technical journals, holds eight patents, and has made numerous presentations in technical conferences. He has authored *Electromagnetic Fields and Waves* (Englewood Cliffs, NJ: Prentice-Hall, 1992), edited the *CAEME Software Books Vol. I* (1991), and *CAEME Software Books Vol. II* (1994), and has edited the four other books *Microwave Processing of Materials* (Mater. Res. Soc., 1990, 1992, 1994, and 1996). He edited two special issues of the *Journal of Microwave Power* ("Electromagnetics and Energy Applications," Mar. 1983, and "Electromagnetic Techniques in Medical Diagnosis and Imaging," Sept. 1983). He also edited a special issue of the *ACES Journal* on computer-aided electromagnetics education and the proceedings of both the 1995 and 1996 International Conference on Simulation and Multimedia in Engineering Education. He is the editor of *Computer Applications in Engineering Education* (CAE) (New York: Wiley). His research interests are in the areas of computational electromagnetics, antenna design, propagation models for wireless communications, microwave processing of materials, biological effects of electromagnetic radiation, and the development of multimedia applications.

Dr. Iskander is a Fellow of the IEEE and a member of the National Research Council Committee on Microwave Processing of Materials. He was an elected member of the Antennas and Propagation Society (IEEE AP-S AdCom) from 1996 to 1999. He was a member of the WTEC Wireless Panel, which visited many of the wireless companies in Europe and Japan to assess the U.S. competitiveness in this technology. He was the general chairman of the 1996 Frontiers in Education Conference sponsored by the IEEE Computer and Education Societies and the general chair for the 2000 IEEE IEEE AP-S International Symposium and URSI meeting. He was an associate editor for the IEEE TRANSACTIONS ON ANTENNAS AND PROPAGATION (1995–1998) and an associate editor of the *IEEE Antennas and Propagation Magazine*. He was a Distinguished Lecturer for the IEEE AP-S (1994–1997) and, during his tenure, he gave lectures in Brazil, France, Spain, China, Japan, and at a number of U.S. universities and IEEE chapters. He was the recipient of the Curtis W. McGraw American Association for Engineering Education (ASEE) National Research Award for outstanding early achievements, the ASEE George Westinghouse National Award for innovation in engineering education, and the 1992 Richard R. Stoddard Award presented by the IEEE Electromagnetic Compatibility (IEEE EMC) Society.